

Rheology, durability, and mechanical performance of sustainable self-compacting concrete with metakaolin and limestone filler

Gemma Rojo-López^a, Belén González-Fonteboá^{a,*}, Fernando Martínez-Abella^a, Iris González-Taboada^b

^a School of Civil Engineering, Department of Civil Engineering, University of A Coruña. E.T.S.I. Caminos, Canales, Puertos, Campus Elviña s/n, 15071 La Coruña, Spain

^b Ministry of Transport, Mobility and Urban Agenda, Paseo de la Castellana 67, 28071 Madrid, Spain

ARTICLE INFO

Keywords:

Supplementary cementitious materials
Material efficiency
Plastic viscosity
Yield stress
Resistivity
Ultrasonic pulse velocity

ABSTRACT

This study analyzed the performance of self-compacting concrete with a paste composition that includes limestone filler and metakaolin replacing cement to design binary (75% cement and 25% limestone filler) and ternary binders (60% cement, 25% limestone filler and 15% metakaolin). Furthermore, to analyze the effect of the solid volume fraction (volume of sand and coarse aggregate) on concrete rheology, the concretes were designed using four volumes of paste (350 l, 400 l, 450 l and 500 l). Rheological tests were performed at three resting times to measure the viscosity and yield stress over time. The results indicated that the viscosity decreased by 43.3% when the cement was replaced by limestone filler and increased by 73.1% when the cement was replaced by 15% metakaolin while maintaining the limestone filler. These values were obtained as 27.6% and 62.2%, respectively, when the yield stress was analyzed. In addition, the hardened properties (mechanical behavior and durability) were studied by measuring the strengths at 28 days, as well as the electrical resistivity and ultrasonic pulse velocity over time. In this case, at 28 days the use of binary binder reduces the strength and resistivity (about 20%) and the employment of ternary binder reduces strength (15%) while increases the resistivity up to the double (when compared to the 100 C concrete). Moreover, to measure the efficiency of the concrete, a material index was designed that considers the fresh behavior, mechanical performance, durability, cost, and environmental impact. Self-compacting concretes with ternary binders provided the highest indices. The use of alternative materials, particularly metakaolin has been proven to be a good option to enhance concrete sustainable performance.

1. Introduction

Self-compacting concrete (SCC) presents a workability of a high-performance concrete [1]. Compared to a vibrated concrete, it shows a different fresh behavior [2,3], which is defined by its fluidity (measured through rheology). To achieve self-compacting behavior, SCC is frequently designed to exhibit a rather high paste volume, which implies high consumption of cement and natural resources. Furthermore, cement production is responsible for 5–7% of CO₂ emissions, as 1 ton of cement emits 900 kg CO₂ into the

* Corresponding author.

E-mail addresses: gemma.rojo@udc.es (G. Rojo-López), bfonteboa@udc.es (B. González-Fonteboá), fmartinez@udc.es (F. Martínez-Abella), gonzalez.iris@gmail.com (I. González-Taboada).

<https://doi.org/10.1016/j.cscm.2022.e01143>

Received 10 March 2022; Received in revised form 26 April 2022; Accepted 7 May 2022

Available online 11 May 2022

2214-5095/© 2022 The Author(s). Published by Elsevier Ltd. This is an open access article under the CC BY-NC-ND license (<http://creativecommons.org/licenses/by-nc-nd/4.0/>).

atmosphere [4].

In recent years, efforts to achieve more efficient cement-based materials have opened up the possibility of using supplementary cementitious materials (SCMs). SCM can be pozzolanic, such as fly ash [5], granulated blast furnace [6], metakaolin [7] or silica fume [8]; or non-pozzolanic, such as limestone filler [9], granite powder [10], marble powder [11] or rubber powder that produces binary, ternary, or quaternary binders. The use of SCM directly affects concrete workability, mechanical performance, and durability.

To understand the rheological behavior of concrete with SCMs, an in-depth knowledge regarding the characteristics of the materials is required, as certain factors, such as, particle size distribution, morphology, and texture have a strong influence [12]. Vance et al. [12] studied the influence of the particle size distribution (PSD) of limestone powder on the rheological behavior and reported that coarse limestone filler decreased the rheological parameters (as it increased the particle spacing); in contrast fine limestone powder resulted in higher yield stress and plastic viscosity (as it increased packing density, resulting in a decrease in interparticle spacing). However, the same authors found that when blended suspensions (Portland cement + limestone filler) were prepared with the same PSD, the use of limestone negligibly affected the plastic viscosity, although it decreased the yield stress [13]. Gesoğlu et al. [5] found that the use of limestone filler and marble powder increased SCC viscosity. Consequently, when analyzing binary blends of cement and metakaolin, the authors concluded that an increase in the replacement rate resulted in an increase in both the rheological parameters [12,14]. This is attributed to the high specific surface area and the tendency of the fine part of metakaolin to agglomerate [12]. Furthermore, an analysis of ternary blend cement with limestone filler and metakaolin [12] where electrostatic forces act by modifying interparticle spacing, concluded that yield stress is reduced as the fine limestone filler content is increased. However, other studies [15] found that the use of metakaolin in limestone cement concrete reduce yield stress while plastic viscosity is increased.

The use of non-pozzolanic materials replacing a significant level of cement usually results in a reduction in the mechanical performance as, in these cases, the physical effects do not compensate the chemical activity of the cement substituted. However, pozzolanic SCMs can counteract this effect [14]. In this regard, the ultrasound pulse velocity is a good indicator of the compressive strength of concrete, as the propagation velocity primarily depends on its density and elastic properties. Concrete durability and its resistance to reinforcement corrosion are primarily influenced by the pore structure and characteristics of the pore solution [16]. The use of binary and ternary binders improves these characteristics. Duc-Hien et al. (2018) [17] found that mixes with sugarcane bagasse ash slag and ground blast furnace slag in binary and ternary binders presented a low risk of corrosion after 28 days.

Finally, to evaluate the sustainability of concrete with binary and ternary binders more accurately, economic and environmental aspects should be considered. For this purpose, different methodologies (found in the literature) can be used with certain being complex [18] whereas others are simple and can be easily used by concrete producers [10].

1.1. Objectives

Although many publications discuss the use of different mineral additions [19], there is lack of data on the use of ternary cement mixes with limestone filler, metakaolin and Portland cement at the level of concrete. Most of works that deal with these supplementary cementitious materials in ternary cement systems analyze the behavior in mortars or cement pastes [20–22] but the works that deal with concretes are scarce [15].

The analysis of the rheological behavior of different cement systems at the level of concrete, using a concrete rheometer, is also a novel approach as most of the research works employ only industrial tests (as V-funnel or slump flow) [23]. The study of the relationship between rheological parameters and solid volume fraction comparing different cement systems is also scarce in the literature [13,24]. It is well known that the inclusion of SCM in concrete produces important changes in its rheological behavior and the structural build-up of the mixes. Although no consensus exists in the literature regarding their effects, the physical and chemical characteristics of the supplementary material used and the relationships they develop with cement particles during the mixing process are the determining factors affecting the fresh behavior of the mixture. Thus, a broad characterization of the material is important for fully understanding these effects.

Regarding hardened behavior, the influence of the paste volume content in concrete compressive strength, UPV or ER is also limited and some authors have suggested that more works are needed in this regard [25].

Finally, to ensure the sustainable behavior of the new concrete, some indexes that takes in account not only fresh behavior, but also mechanical performance and durability must be studied when designing this type of concrete. This work covers fresh, hardened and durability properties of the concrete. This allows the authors to develop an analysis of the efficiency of the concrete considering all these important aspects together.

Therefore, the primary objective of this study was to evaluate the effect of binary and ternary binders on the performance of SCC. First, the fresh state behavior was analyzed using rheology as a tool of science, which facilitated the study of interactions between the physical and chemical characteristics of the SCMs within the paste and concrete upon addition of fine and coarse aggregates. Second, the efficiency of SCC with binary and ternary binders was measured and compared. The hardened behavior was determined using destructive and non-destructive tests. Finally, the fresh state behavior, mechanical and durability performance, cost, and environmental impact were considered in the material efficiency assessment.

2. Experimental program

2.1. Raw materials characterization

Three powder materials were used in this study: Portland cement labelled CEM I 52.5 N-SR5 (C), limestone filler (F), and

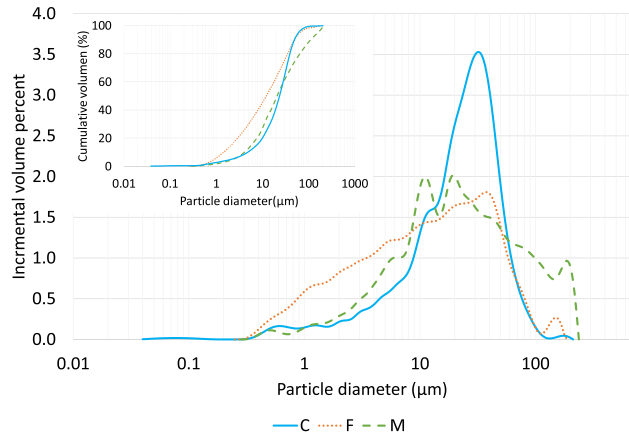


Fig. 1. Grading curves of powder materials.

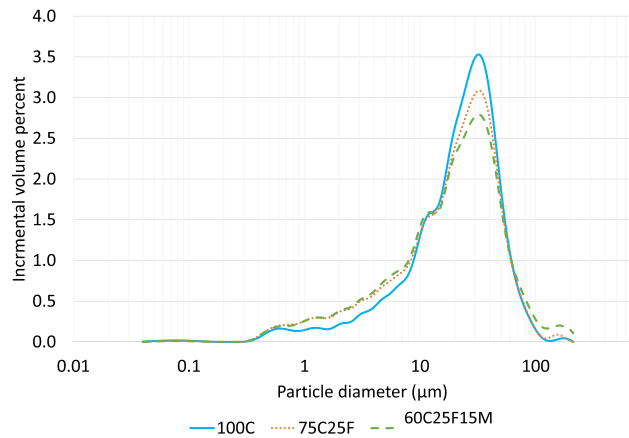


Fig. 2. Grading curves of blended binders.

Table 1
Physical properties of powder materials and blended systems.

	C	F	M	75C25F	60C25F15M
Specific density (g/cm ³)	3.11	2.64	2.55	2.99	2.91
SSA _{BET} (m ² /g)	1.36	1.44	4.25	1.38	1.81
SSA _{BET} (m ² /m ³)	4.23E+ 06	3.79E+ 06	10.8E+ 06	4.13E+ 06	5.27E+ 06
SSA _{PSD} (m ² /m ³)	0.66E+ 06	1.413E+ 06	0.675E+ 06	1.04E+ 06	1.00E+ 06
SSA _{PSD} (m ² /g)	0.286	0.535	0.265	0.349	0.3451
D ₁₀ (μm)	4.91	1.46	4.18	4.05	3.938
D ₅₀ (μm)	23.69	12.24	20.96	20.82	20.42
D ₉₀ (μm)	49.77	50.21	112.17	49.88	59.24
Particle density - N _{PSD}	23	55	19	31	30.4

metakaolin (M) as SCM in binary and ternary cementitious blends. To compare the effect of SCM on concrete properties, F and M were used by partially replacing cement by volume, yielding three blended cementitious systems: 100 C (100% cement), 75C25F (75% cement and 25% limestone filler), and 60C25F15M (60% cement, 25% limestone filler, and 15% metakaolin).

The particle size distribution (PDS) of the systems, measured using a laser diffractometer, is shown in Fig. 1 and Fig. 2. The D90, D50, and D10 parameters, along with the specific density are presented in Table 1. As expected, limestone filler is thinner than cement or metakaolin.

The nitrogen gas adsorption technique was used to calculate the specific surface area (SSA_{BET}). Further, using the PDS and assuming a spherical shape without pores for the particles, the specific surface area per unit volume (SSA_{PSD}) and the particle density (N_{PSD}) was estimated following Navarrete et al. [24].

Table 2
Chemical composition of powder materials (XRF).

% by mass	C	F	M
SiO ₂	18.9	1.5	58.0
Al ₂ O ₃	6.3	0.45	36.8
Fe ₂ O ₃	2.7	0.22	1.2
CaO	59.9	55	0.075
K ₂ O	1.9	0.12	2.1
MgO	1.6	0.49	0.18
SO ₃	3.5	0.17	0.058
LOI	4.3	41.9	0.7

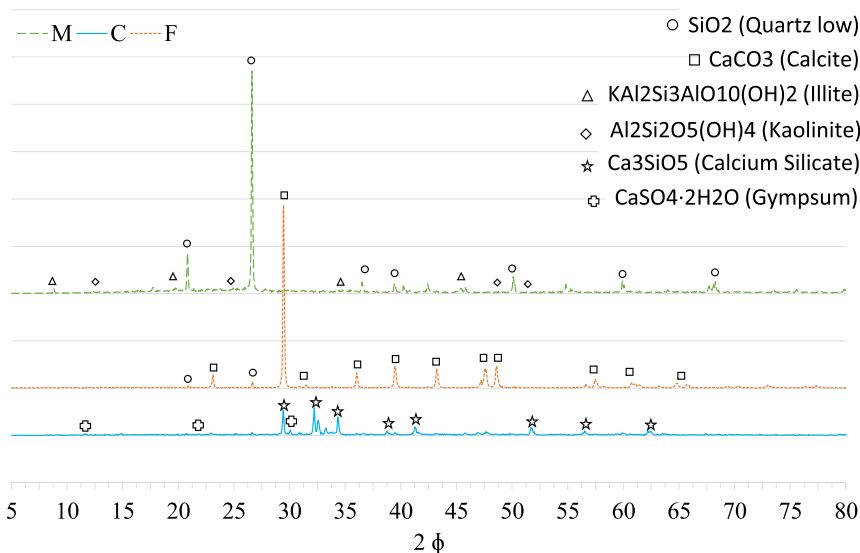


Fig. 3. X-Ray Diffraction.

The chemical composition was determined by X-ray fluorescence (XRF), presented in Table 2. Further, phase identification was performed via X-ray diffraction (XRD) to identify the presence of different amounts of crystalline phases (Fig. 3) in each powder. Scanning electron microscopy (SEM) images of C, F, and M are shown in Fig. 4.

Fig. 1 shows that the PSD of the powder materials are different. Limestone filler presents finer particles than cement or metakaolin. However, on comparing the particle distribution of cement and metakaolin, it is evident that metakaolin presents finer and coarser particles than cement, as the volume of the middle-sized particles is smaller. This was confirmed by SEM images (Fig. 4.b), where the presence of fine particles in the limestone filler image was clear. As shown in Fig. 2, the 75C25F and 60C25F15M mixtures exhibited similar particle size distributions because of the limestone filler. Both mixtures have more fine particles than cement-only systems (100 C).

Differences between SSA_{BET} and that calculated using the PSD were 6.4, 2.7, and 15.9 times those calculated with the particles size distribution considering spherical particles without pores for cement, limestone filler and metakaolin, respectively. The highest difference was observed with the metakaolin, implying that the particle shape of this material was considerably different from the spherical shape. Further, SEM images (Fig. 4) show that the high specific surface value of metakaolin is due to its irregular shape, rough surface, and high open porosity with layers in parallel geometry, which facilitates the adsorption of N₂ and provides high values of SSA_{BET} . The calcination process employed for the metakaolin was the “fluidized bed process,” which according to the literature [26] generates angular and salient shape particles. However, in the SEM images, certain particles were observed to exhibit perfect roundness. In the SEM images, the limestone filler particles appeared smooth and irregular. In contrast, cement particles were irregular in shape and the texture was not as rough as that of metakaolin, nor as smooth as that of limestone filler.

According to XRF analysis, M presents a SiO₂/Al₂O₃ ratio of 1.58, implying that it is a metakaolin with low impurity content, considering that a ratio equal to 1.18 is considered pure M [26]. This is in accordance with the XRD analysis, which showed the presence of kaolinite and detectable amounts of illite and quartz. In addition, this is consistent with the results of Cassagnabère et al. (2013) [26] who concluded that the employment of the fluidized process results in metakaolin presenting a less amorphous structure in the area of the halo centered at $2\theta = 27.07^\circ$. To confirm the pozzolanic activity of the metakaolin, it was measured following the French standard NF P18–513 [27]. The lower limit to be considered as pozzolanic is 650 mg of Ca(OH)₂ [28] and the results obtained with metakaolin used in this work provide a value of 946 mg of Ca(OH)₂; hence, metakaolin is considered to be a pozzolanic material.

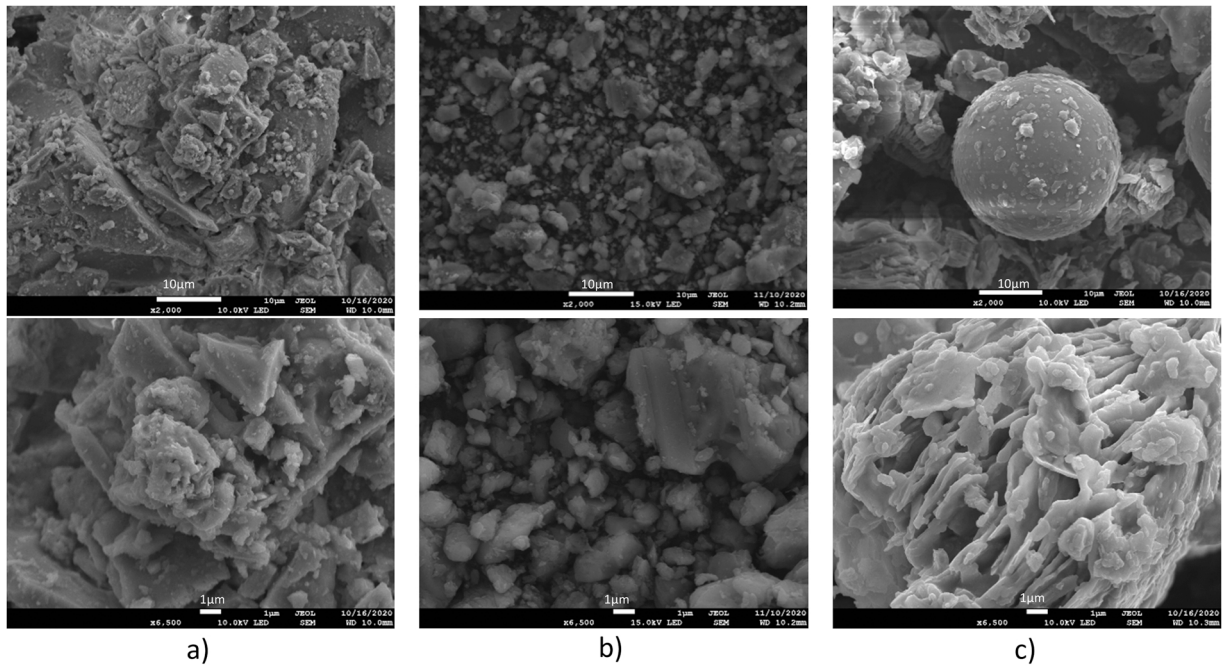


Fig. 4. a) Cement, b) Limestone filler, c) Metakaolin.

Table 3
Properties of aggregates.

	FA	CA
Density (g/cm ³)	2.72	2.81
Water absorption 24 h (%)	1.05	0.63
Los Angeles coefficient (%)	–	18
BET Surface (m ² /g)	73	–

Table 4
Mixture proportions (1 m³).

Paste level (l)	Binder (%)	V _w /V _b	Dosage (l/m ³)						
			CEM	LP	M	FA	CA	Super	Water
350	100 C	1.1	165.78			325.00	325.00	1.86	182.36
	75C25F		124.50	41.50				1.39	182.60
	60C25F15M		99.60	41.50	24.90			1.39	182.60
400	100 C	1.1	189.47			300.00	300.00	2.12	204.41
	75C25F		142.29	47.43				1.59	208.69
	60C25F15M		113.83	47.43	28.46			1.59	208.69
450	100 C	1.1	213.15			275.00	275.00	2.39	234.46
	75C25F		160.07	53.36				1.79	234.78
	60C25F15M		128.06	53.36	32.01			1.79	234.78
500	100 C	1.1	236.83			250.00	250.00	2.65	260.52
	75C25F		177.86	59.29				1.99	260.86
	60C25F15M		142.29	59.29	35.57			1.99	260.86

Finally, fine (FA) and coarse (CA) crushed aggregates (limestone) were used, with nominal size of 0–4 and 6–12 mm. Their physical properties are presented in [Table 3](#):

The maximum packing fraction of the aggregates was experimentally measured using the method described in the literature [29]. It was measured considering the combination of fine and coarse aggregates according to the CA/FA ratio defined in the mixture proportions, yielding a value of 0.73.

Tap water and a polycarboxylate superplasticizer (Sika ViscoCrete-3500) were used in the mixtures.

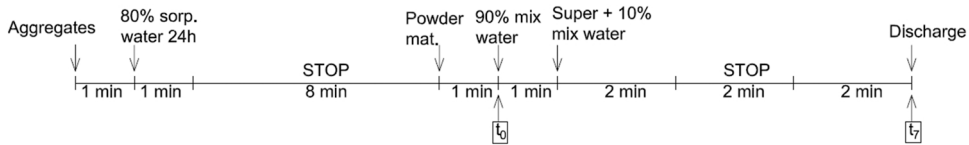


Fig. 5. Mixing protocol.

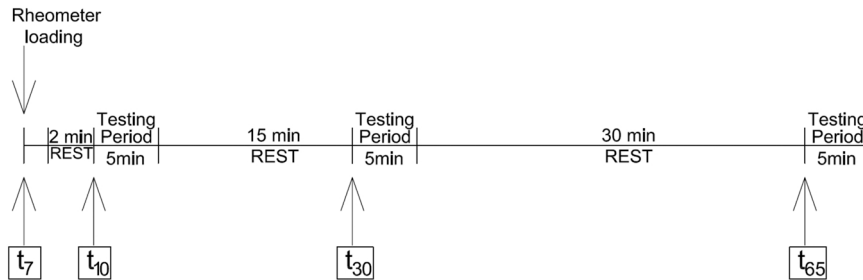


Fig. 6. Testing protocol.

2.2. Concrete mixes

SCCs were designed varying the solid volume fraction (that is the volume of sand and coarse aggregate) or, accordingly, the paste volume (volume of paste in 1 m^3). Therefore, four different paste levels (350, 400, 450, and 500 liters) were employed in the concrete mixes. These pastes were designed using the three blended cementitious systems: 100 C, 75C25F, and 60C25F15M.

The mixture parameters of the concrete are listed in Table 4. All mixtures were prepared with the same water-to-binder volumetric ratio (V_w/V_b of 1.1), coarse-to-fine aggregate volumetric ratio (CA/FA of 1.0), and superplasticizer dosage (1.12%).

To avoid aggregates from absorbing water from the mix, they were dry homogenized in the mixer for 1 min and then mixed with the water calculated to compensate their absorption at 10 min for another minute. After that, the mixer was stopped for 8 min and then rotated again for 1 min introducing the powder materials. In this manner, the aggregates were 10 min in contact with the water that compensates their absorption at 10 min.

Concretes were made using batches of 36 l that were prepared in a vertical-axis mixer. The mixing protocol is illustrated in Fig. 5. In this figure t_0 is the time of cement-water contact (the reference time) and t_7 is the time when the concrete is taken off the mixer and introduced in the rheometer (7 min from t_0).

2.3. Methods

After discharging the concrete from the mixer in t_7 (Fig. 5), it was immediately introduced into the rheometer, and its rheological behavior was measured following the steps described in Fig. 6.

The rheological properties of the studied concretes were determined at different ages, that is, 10 (t_{10}), 30 (t_{30}), and 65 (t_{65}) min, from the time of cement-water contact (the reference time, t_0). These testing times (age of the mix) corresponded to three different resting periods: 2, 15, and 30 min

Two rheological tests were performed at each testing time using a portable rheometer with vane geometry, ICAR rheometer: the stress growth test (SGT) and flow curve test (FCT). SGT was performed twice under two conditions: first *undisturbed*, immediately after the resting time, and thereafter *disturbed*, immediately following the first one. In this test the constant rotational speed was 0.025 rps and the test was stopped after 60 s, once the peak torque was reached. Then, the vane was removed, the concrete remixed with a shovel and the disturbed SGT started (using the same speed and duration as before). Subsequently, the FCT was performed. In this test a rotational speed of 0.5 rps was applied for 20 s and then the speed was decreased in seven steps to 0 rps. The torque was measured in the descending steps of the test. The time required to perform these tests was 5 min

For each testing time wherein rheological characteristics of the mixtures were analyzed, the slump flow test according to EN 12350-8 [30] was developed to measure the spread diameter and T500 parameters.

After the rheological tests were performed, five cylindrical specimens ($150 \times 300 \text{ mm}$) were cast to control the hardened-state properties. While three specimens were used to measure the compressive strength according to UNE-EN 12390-3 [31] the other two specimens were used to evaluate the tensile splitting strength [32] at 28 days of age.

Three additional cylindrical samples ($100 \times 200 \text{ mm}$) were cast to evaluate their Electrical Resistivity (ER) and ultrasonic pulse velocity (UPV). The UPV was performed with the Pundit equipment and 54 kHz type transducers. The surface ER was measured using the Wenner 4 probe method following UNE 83988-2:2014 [33]. Both tests were conducted on the same specimen, always following the same sequence: measurement of ER in six generatrices followed by measurement of UPV between the top and bottom surfaces of the sample. The test specimens were maintained in water up to the testing days (2, 7, 14, 21, 28, 56, 70, 112, and 126 d).

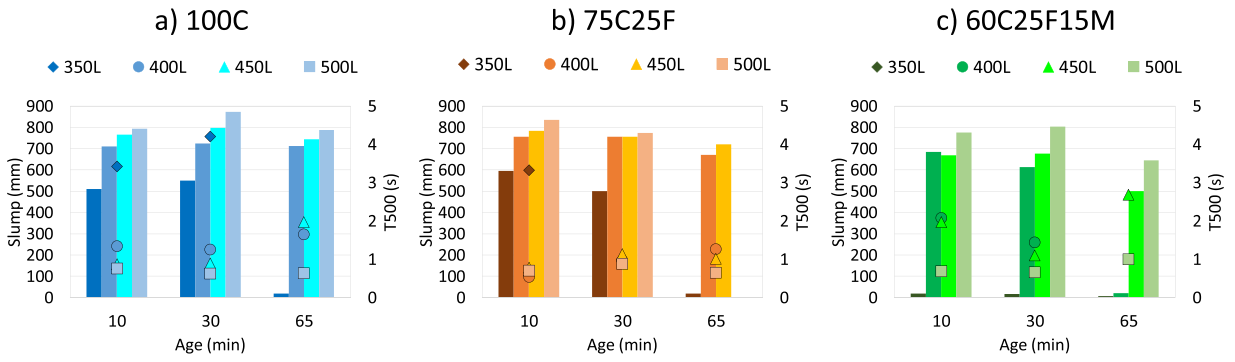


Fig. 7. Slump flow test results.

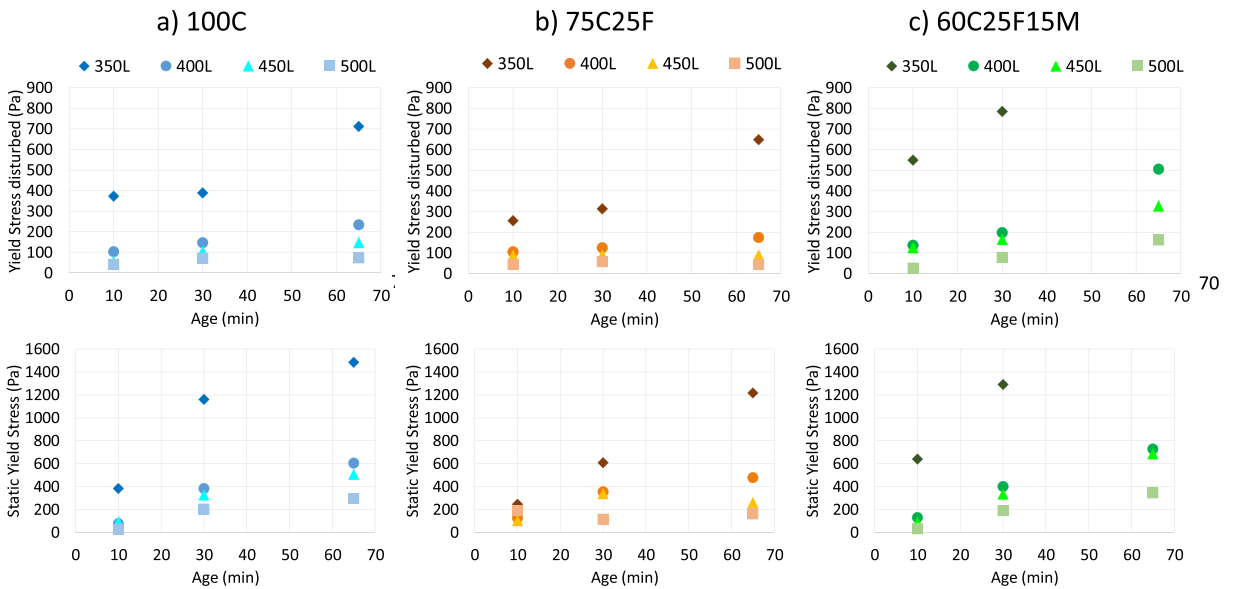


Fig. 8. Static yield stress disturbed (top) and undisturbed (bottom).

3. Analysis of fresh state behavior

3.1. Slump flow results

The slump flow results are shown in Fig. 7. To consider a suitable self-compacting concrete, limits were established according to the European Guidelines for Self-Compacting Concrete specifications, production, and use [34]. Considering these limits, when only 350 l of paste is used, many mixes were observed to lose their self-compacting behavior; 60C25F10M was not self-compacting at any time, 75C25F at 30 and 65 min, and 100 C at 65 min. In addition, with 400 l of paste, only the mix 60C25F10M at 65 min did not fulfil the requirements.

As expected, the T500 increased over time as the paste content decreased. Self-compacting mixes with 400, 450, or 500 l of paste yielded a low value of T500 (lower than 2 s), which showed minimal evolution with time; however, mixes with only 350 l of paste are clearly more sensitive over time. This test is very operator sensitive; therefore, analyzing the effect of the paste composition is challenging. However, when metakaolin was added, the T500 values slightly increased.

The spread diameter results show that an increase in the paste content resulted in an increase in this parameter. This increase was significant when the paste content increased from 350 to 400 l, showing that the concrete with 100 C and 75C25 had an increment of 40% and 25%, respectively. However, when the paste content increased from 400 to 500 l, the spread diameter increased by approximately 7% (100 C and 75C25F). Further, analyzing the effect of time, a reduction trend of the spread diameter was observed, which was more pronounced when the paste content was low. In contrast, for high paste content at early ages, the spread diameter was similar, regardless of the paste composition. However, at later ages or when the paste content was only 350 l, the concrete with 60C25F15M exhibited the lowest values of spread.

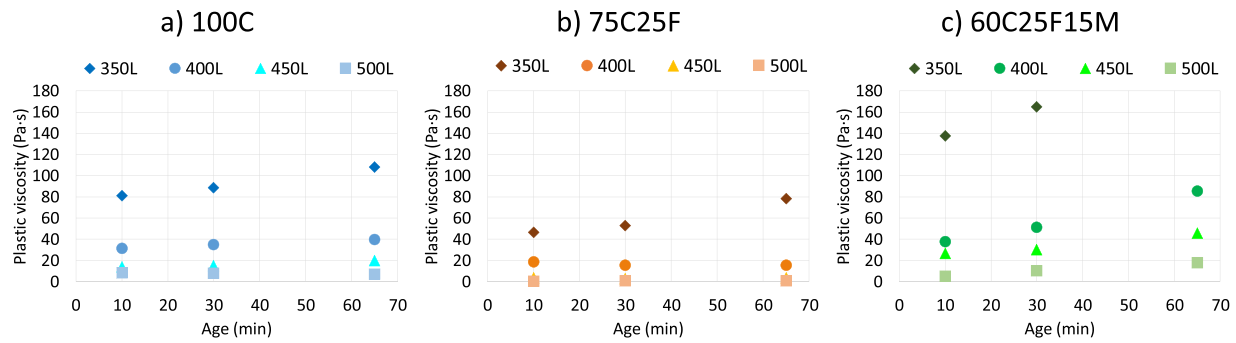


Fig. 9. Plastic viscosity evolution with time.

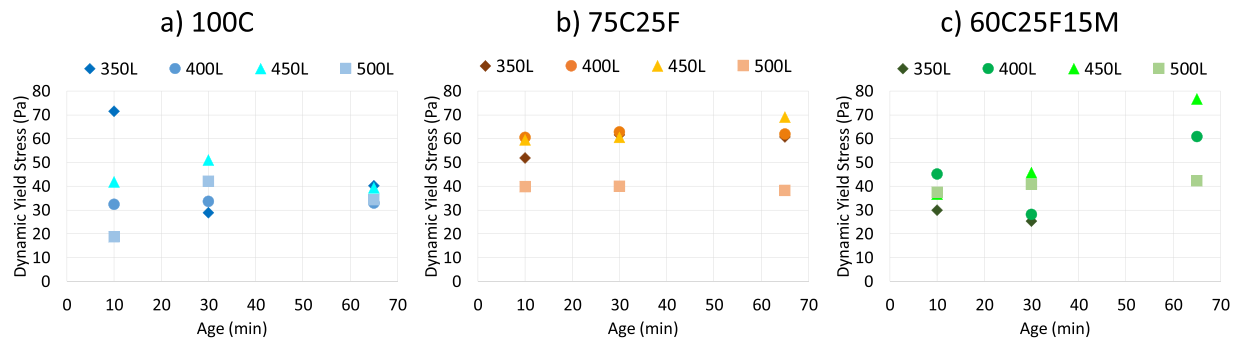


Fig. 10. Dynamic yield stress evolution with time.

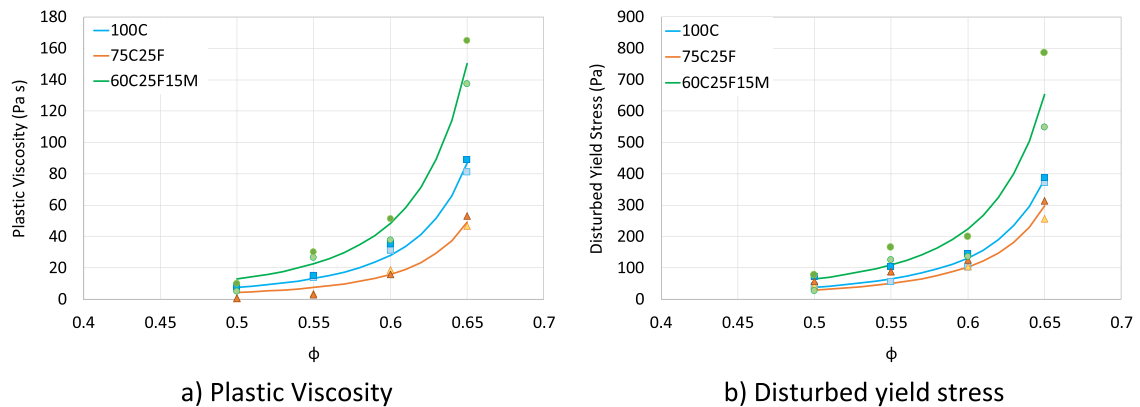


Fig. 11. Rheological parameters vs. solid volume fraction.

3.2. Stress growth test results

The SGT results are discussed in this section. This test was performed twice, under both undisturbed and disturbed conditions, at the following testing ages: 10, 30, and 65 min

At 65 min, the mixtures produced with ternary binders and 350 l paste lost SCC characteristics, and the rheological test could not be performed. Furthermore, certain level of segregation was observed in a few of the samples in concrete with a paste volume of 500 l.

The static yield stress decreases as the paste content increases. This rheological parameter is always higher under undisturbed conditions than under disturbed conditions, as expected. Further, the differences between both measurements, undisturbed and disturbed, appear to be smaller for high paste contents (500 and 450 l) than for low paste contents (400 and 350 l).

As shown in Fig. 8, the replacement of cement with limestone filler decreased the static yield stress in comparison to the cement only mixture. However, the use of metakaolin at 15% (replacing cement and maintaining the limestone filler at 25%) resulted in an increase in the rheological properties (yield stress), even exceeding the value obtained with the cement-only base mixture. This implies that a binary blend based on cement and limestone filler improves flowability, whereas the introduction of metakaolin in the ternary cement reduces the fluidity of the mixture.

Regarding the evolution over time, it is evident that for the 10 min measurement, where the mixture was at rest for just two min in the rheometer, as expected, the values for both the undisturbed and disturbed states were essentially the same. An increase in the static yield stress for both testing states was observed in all the mixtures over time.

3.3. Flow curves: dynamic yield stress and plastic viscosity results

For the flow curves (in relative units), the Bingham model was applied using the seven data points obtained from the FCT at each of the seven steps in the descending ramp of the testing protocol. Certain authors have concluded that the Bingham model estimates higher yield stress values than other models [35] and the use of models such as Hershel Bulkeley or Eyring have provided better adjustments for the study of cement pastes [36]. However, in this study, the Bingham model was used to calculate rheological parameters in absolute units.

With regard to viscosity over time (Fig. 9), this property remains constant for high paste contents and mixtures with cement only or cement and limestone filler. Viscosity differences were more noticeable in the 350 l concrete series. The viscosity values showed an increasing tendency when metakaolin was incorporated, whereas the lowest values were obtained for mixtures with cement and filler. Moreover, in all systems the viscosity decreases as the paste content increases.

Regarding the behavior over time, the dynamic yield stresses (Fig. 10) showed minimal change for paste contents of 400, 450, and 500 l when cement only, or cement and limestone filler were used. This is because only reversible phenomena are occurring. However, an increase over time was observed in the values of both parameters for mixtures with cement, filler, and metakaolin, particularly at 65 min, and for concrete with a low paste content. This implies that an irreversible phenomenon occurs.

These results indicate that, for all concretes, the dynamic yield stress does not change for up to 30 min, implying that the concrete is in the dormant period and hydration reactions can be neglected (considering that only reversible phenomena occur). As occurs with the viscosity, the dynamic yield stress decreases as the paste content increases.

3.4. Rheological parameters and solid volume fraction

To better analyze the effect of the paste content and composition on the rheological behavior of concrete, curves for the solid volume fraction as a function of the rheological parameters were plotted using the results up to 30 min (considering that concrete is in the dormant period and hydration reactions can be neglected). Fig. 11 shows the rheological parameters of concretes with different types of powders at ages of 10 and 30 min when the aggregate volume is modified. Empty bullets correspond to the results at 10 min

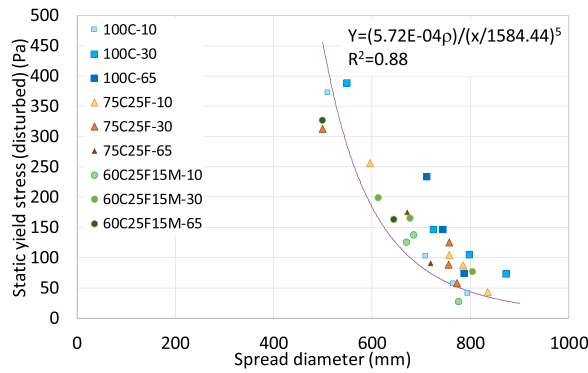


Fig. 12. Relationship between Static Yield Stress and slump flow.

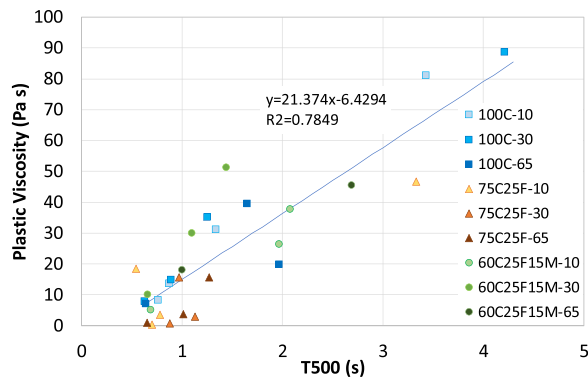


Fig. 13. Relationship between T500 and Plastic Viscosity.

and full bullets with the values obtained at 30 min.

The values obtained indicate a clear increment in the rheological parameters when the solid volume fraction rises. They also show that the viscosity decreases when the cement is replaced by limestone filler and increases when the cement is replaced by metakaolin while maintaining the limestone filler. Comparing 75C25F concrete with 60C25F15M, it is evident that the inclusion of metakaolin sharply increases both rheological parameters.

According to Table 1, the limestone filler system 75C25F displays a higher specific surface area and particle density than the 100 C system, implying that the separation distance between particles is lower. This results in an increase in the physical interaction between the particles, thereby increasing the rheological parameters. However, both yield stress and viscosity are lower at 75C25M than at 100 C; therefore, colloidal forces must be considered. Certain forces are repulsive, that is, electrostatic forces between similarly charged surfaces, while others are attractive, such as van der Waals and electrostatic forces between opposite charges on the surface of the particles. When using different powder materials, the van der Waals forces can be repulsive; however, when using only cement, these forces are always attractive [13]. Furthermore, because of the similar charges on the surfaces of the cement particles, the electrostatic forces are repulsive. Depending on the magnitude of the generated forces, if attractive forces dominate the system [37], flocculation occurs and the rheological parameters increase in value. In contrast, if repulsive forces rule, then a stable colloidal system is produced and the rheological parameters are lower. The solid loading influences, which is the dominant force, such that when a certain solid volume fraction exceeds the Van der Waals force rule, whereas below this concentration, the repulsive forces control the behavior of the mixture. Regardless, the particle size in a cement system is quite large; therefore, Brownian forces were not considered in this study. Consequently, the reduction in both the apparent yield stress and plastic viscosity with the incorporation of limestone into the concrete paste is because of the reduction in the number of flocculated cement particles, as its inclusion increases the repulsive forces while reducing the cement particle connections. In this case, this factor dominated the particle spacing, resulting in the 100 C system presenting higher rheological parameters than the 75C25F system.

Analyzing the system with limestone filler, it was observed that 75C25F and 60C25F15M presented similar particle densities, although their specific surface areas were very different and higher in the metakaolin system. Metakaolin has a very high specific surface area and a rough and irregular structure (sometimes layered like kaolinite, with elongated particles), indicating that it increases the water demand, reduces the interparticle distance, and promotes particle jamming. These properties have enabled concrete with metakaolin to completely counteract the effect of limestone filler and consequently present the highest values of both yield stress and plastic viscosity. These results agree with those obtained by other authors analyzing mortars or pastes with metakaolin [38]. [38] reviewer observed, at the level of a mortar, that the substitution of cement with M leads to an increase in the plastic viscosity at a

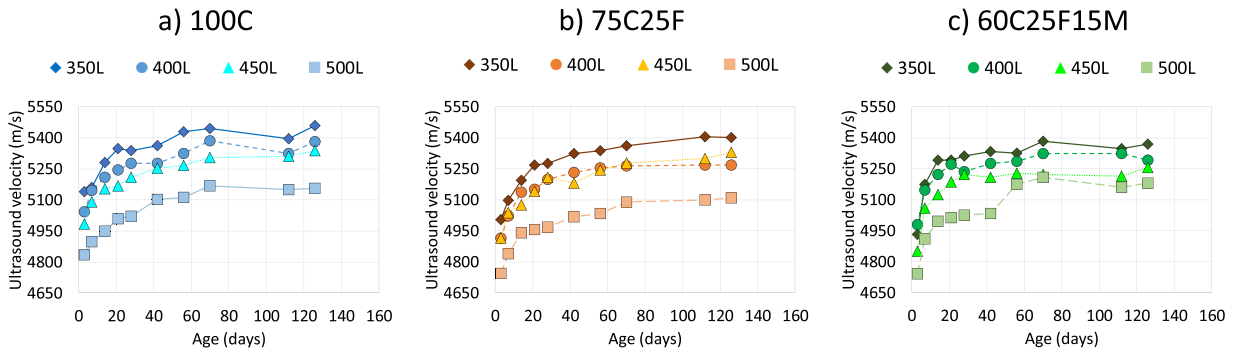


Fig. 14. Ultrasound pulse velocity over time.

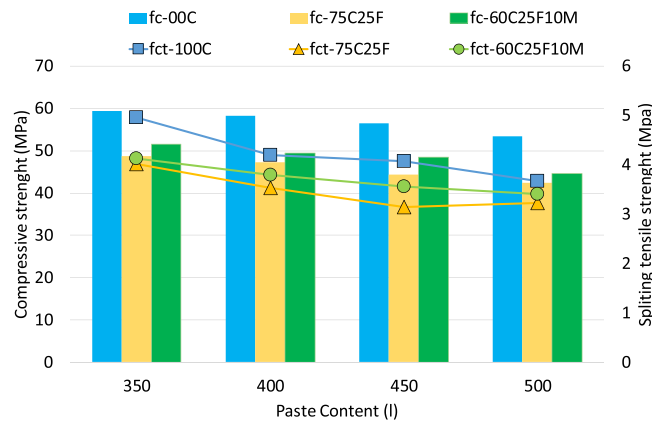


Fig. 15. Compressive and splitting tensile strength (28 days).

constant or even increasing the dosage of superplasticizer. The yield stress also rises with the inclusion of metakaolin when the superplasticizer is kept constant.

Finally in Fig. 12 and Fig. 13 the relationships between the yield stress and slump flow and the plastic viscosity and T500, respectively, are plotted. The slump flow test is an industrial test that analyzes both the yield stress and viscous behavior of fresh concrete; therefore, the measurements of spread and T500 are related to different rheological parameters. In the figures, the relationship shown by all mixes, regardless of the cementitious composition or paste content, is similar.

The relationship between the yield stress and slump flow test diameter is a function of the material density and is similar to that obtained in other studies for SCC [35,36]. In addition, a good relationship was found between viscosity and T500.

4. Analysis of hardened behavior

To analyze the hardened behavior, the evolution of the pulse velocity, compressive strength, and splitting tensile strength at 28 days were measured. The evolution of ER was used to measure concrete durability.

4.1. Ultrasonic pulse velocity and strengths

Fig. 14 shows the evolution of the ultrasonic pulse velocity (UPV) of all mixes. This parameter exhibits a high rate of gain at early ages that slows down in a later state; however, certain differences can be observed in different concretes. At early ages, mixes with only cement (100 C) and 60C25F10M exhibited the highest and lowest values, respectively. However, at long ages, the mix with metakaolin and 75C25F exhibited the maximum and minimum velocity values, respectively. In addition, the concretes with a high aggregate content showed higher values of ultrasonic pulse velocity; that is, mixes with only 350 and 500 l of paste always present the highest and lowest values, respectively.

Ultrasonic wave propagation depends on the dynamic elastic modulus, Poisson’s ratio, and density of the medium; therefore, it differs between aggregates and pastes. In addition, the measured value depends on the velocity in each of these systems and their volume content. At a low aggregate content, UPV depends primarily on the velocity in the matrix. In this study, aggregates presented a denser structure than the matrix, thus, the values of UPV were higher in concrete with a higher aggregate content.

Comparing concretes with the same aggregate content, the velocity of the wave depends on the matrix properties, primarily the

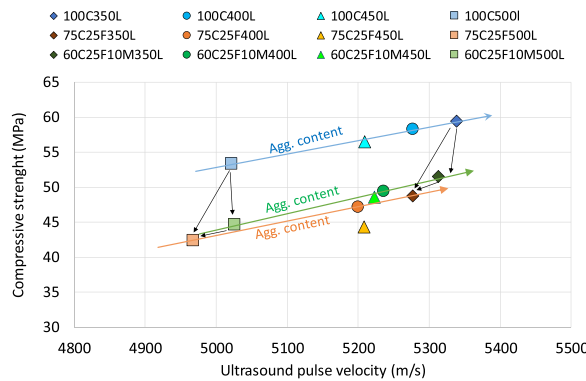


Fig. 16. Compressive strength vs UPV (28 days).

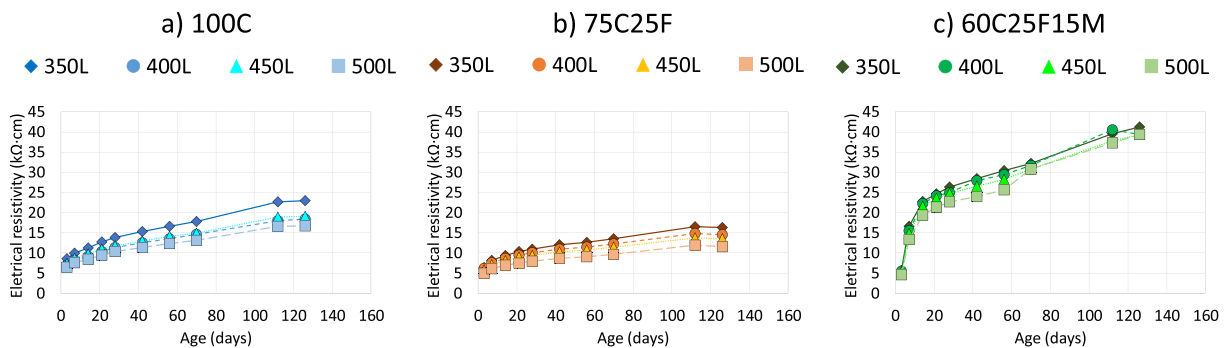


Fig. 17. ER over time.

density of the microstructure, which is related to the hydration process. During setting and hardening, pore refinement of the concrete matrix occurs, and then the UPV grows. The evolution of the UPV exhibited a different reaction in mixes with metakaolin owing to its pozzolanic reaction as was already seen by other authors when studying the compressive strength evolution [39]. While 100 C and 75C25F showed a similar trend in the evolution of ultrasonic velocity, the performance of the 60C25F15M mix was different. In the first days, the rate of gain (the slope of the curves) was high, whereas after 20 days, it slowed down and became similar to the evolution observed at 100 C and 75C25F. After 28 days, the UPV decreases as the paste content increases.

The influence of the paste volume content in concrete compressive strength is complex and limited works has been developed to clarify the reasons behind [35,36]. Fig. 15 shows the compressive and splitting tensile strengths at 28 days and, in this work, the results indicate that the strength decreases as the paste content increases. This is attributed to the mortar thickness coating the aggregates. When the aggregate volume in the concrete is high the path the crack needs to follow is long, as it has to move around a great number of aggregates. This makes the energy absorbed high. When the volume of the paste is high and the volume of the aggregates is small, the length of the path becomes straighter leading the amount of energy absorbed smaller.

Other researchers have detected the same effect [39–42] and they suggest that more research is needed in order to clarify the reasons for this. For instance, [40] found that, at constant w/c ratio, decreasing the cementitious paste volume, increased the strength and quality of concrete and that this enhancement effect was related to the average thickness of mortar films coating the aggregate. The same effect was detected by [41] that measured an increase of strength as the volume of the paste in the mix decreases.

De Larrard and Belloc [43], funding the same trend, attributed it to the maximum paste thickness which is defined as the mean distance between adjacent coarse aggregates.

When cement is replaced by SCM, the strength decreases. The reduction in the system with limestone filler (75C25F) was approximately 20% for all paste contents. This agrees with the results of other authors [39,44–46] that detected at all ages a reduction in the compressive strength with increasing the limestone filler due to the dilution effect that could not be compensated by the filler effect. However, when metakaolin was added to the mixture, the reduction was lower (approximately 15%) owing to the pozzolanic reaction and to the synergic effect of the combination of limestone filler and metakaolin. Drissi et al. [39] found that metakaolin in combination with limestone filler could bridge the dilution effect of LS at later ages.

Fig. 16 shows that the relationship between compressive strength and UPV at 28 days is different depending on the blended cement used. Upon comparing 100 C and 60C25F10M it is evident that they present (at any aggregate content) almost the same UPV; however, concretes with only cement 100 C provide the highest compressive strength. The use of limestone filler replacing cement contributes to reduction of the volume of voids in the cement paste, hence improves the compactness of the matrix; however, the compressive strength at 28 days when using limestone filler does not exhibit growth to the same extent as in the system with only cement. The

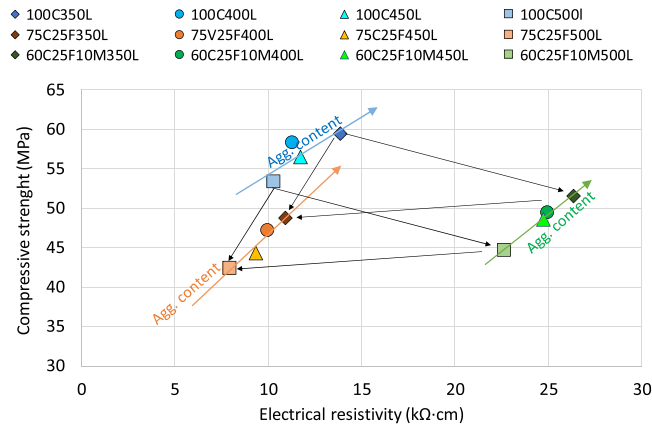


Fig. 18. Compressive strength vs ER (28 days).

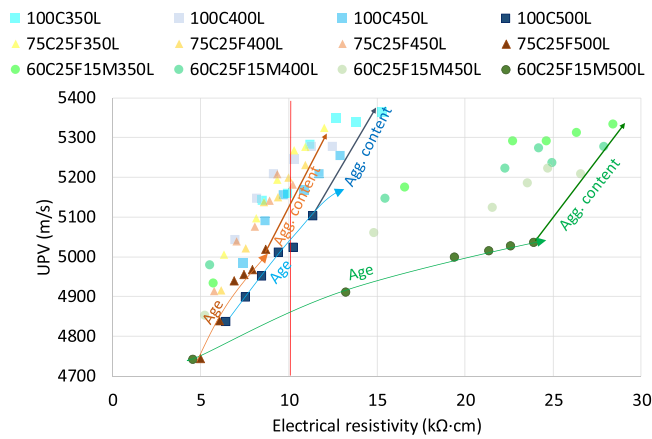


Fig. 19. ER vs UPV at different ages.

differences in this relationship between 75C25F and 60C25F10M are minimal, providing slightly higher UPV and, accordingly, slightly higher compressive strength than the mix with metakaolin. In addition, the influence of the aggregate content is similar in all systems. As the aggregate content increased both compressive strength and UPV increased as well.

4.2. Electrical resistivity

The ER, as shown in Fig. 17, followed the same trend as the UPV; that is, the results show a high rate of gain at early ages (owing to the hydration process) that slows down at later stages. Again, the highest values at early ages are shown by 100 C concretes, with the mix with 60C25F10M showing the best results at later ages. Further, this parameter also increases with increase in the aggregate content.

However, the differences among the concretes are more notable than in UPV because this parameter is more influenced by the pore structure and its connectivity than the UPV or compressive strength. The refinement of the dense structure and the densification of the composite matrix produced by the pozzolanic reaction of metakaolin at later ages results in concretes with this material presenting a different long-term behavior. Thus, the beneficial effect of introducing metakaolin in cement systems is clear. Moreover, for the same UPV, systems with metakaolin provide ER values that are almost twice the resistivity measured in the 100 C or 75C25F system. This is particularly significant for 60C25F10M with 350 l of paste.

Fig. 18 shows that at 28 days, the use of limestone filler reduces both compressive strength and ER; however, on incorporation of metakaolin, although the compressive strength is also reduced, the ER considerably increases. Further, concrete durability can be improved using this material that fills voids wherein primarily the compactness of the matrix producing a pore structure refinement after pozzolanic activity is improved. Upon comparing 100 C and 75F25F, it can be concluded that the system with limestone filler presents lower compressive strength and slightly lower ER.

The influence of the aggregate content was similar in all systems and followed the same trend as that of the UPV. As the aggregate content increased, ER increased as well.

These results indicate that compressive strength is closely related to UPV, but ER is much more sensitive to the compactness of the

Table 5
Corrosion risk levels (ref).

ER	Corrosion risk
$\rho > 200 \text{ k}\Omega \text{ cm}$	Low Corrosion Risk
$200 > \rho > 10 \text{ k}\Omega \text{ cm}$	Moderate Corrosion Risk
$\rho < 10 \text{ k}\Omega \text{ cm}$	High Corrosion Risk

Table 6
GWP and cost for each material.

Material	GWP (kg CO ₂ /kg)	Cost (€/kg)
Cement	0.830 [53]	0.100
Metakaolin	0.09240 [54]	0.425
Limestone filler	0.01905 [53]	0.01
Aggregates	0.00246 [53]	0.01
Water	0.000318 [55]	0
Superplasticizer	0.994 [54]	0.98

matrix obtained by the pozzolanic reaction of the metakaolin.

Fig. 19 shows the relationship between the UPV and ER at different ages. The effect of the hydration process can be observed in this figure. The system with 100 C and 75C25F presents a comparable relationship between UPV and ER, and the slope of the curve that relates these two parameters is similar. As the UPC increases, the ER rises to a similar extent in both systems. However, the system 60C25F10M exhibits a clearly different trend; as the UPV increased, the rate of gain in the ER was considerably high.

ER has been extensively used to estimate concrete durability, because it is related to the transport properties of concrete. According to the literature [47], corrosion risk can be classified into three levels (low, moderate, and high) that are related to the ER values (Table 5).

At short ages, all mixes presented a high corrosion risk, with values under 10 kΩ cm. These values agree with the results of the literature, where, at short ages, the ER is always low [48]. However, from day 7 onwards, mixes with ternary cement obtained values of moderate risk. In most mixes with only cement, it is necessary to wait up to 20 days to overcome the 10 kΩ-cm and mix with 75C25F, and a high quantity of paste (500 L) does not obtain this value. This is consistent with the results of Bagheri et al. [49], where, when using fly ash and silica fume in different replacement percentages concretes with 20% and 30% of fly ash and silica fume, respectively, exhibited ER values twice the ones of the baseline mix at 28 days. Sadrmontazi et al. [50] concluded that the incorporation of silica fume has beneficial effects in the interfacial transition zone owing to the pozzolanic reactions that dismiss the portlandite content and increase the uniformity and density of the matrix and the bond between the matrix and the aggregate.

5. Material efficiency

The correct selection of raw materials for the design of new concrete mixes has recently become important for ensuring that they achieve certain economic benefits that do not compromise the service capacity of structures. The ISO14067 [51] defines carbon footprint as follows: "it is a sum of greenhouse gases emissions and removals in a product system expressed as CO₂ equivalent."

The material efficiency of the concretes designed in this study was studied following the procedure reported in the literature [52]:

$$ME = \frac{w1 \cdot \frac{D_{flow}}{D_{flow,ref}} + w2 \cdot \frac{f_{cm}}{f_{cm,ref}} + w3 \cdot \frac{R_{esis}}{R_{esis,ref}}}{\frac{GWP}{GWP,ref} \cdot \frac{Cost}{Cost,ref}} \quad (1)$$

where D_{flow} , f_{cm} , and R_{esis} are the flow diameter, compressive strength, and resistivity at 28 days, respectively, and represent the material engineering performance, GWP and Cost are the global warming potential and unit cost, respectively, of a given concrete mixture, and $D_{flow,ref}$, $f_{cm,ref}$, $R_{esis,ref}$, GWP_{ref} , and $Cost_{ref}$ are related to the values of a reference mixture or target values established in view of a given practical application. In this study, the reference values established were the averages of the values measured for all mixtures analyzed, and w_i was established as 0.33.

This indicator has been designed to show an increment (higher material efficiency) when the material performance is improved and when the environmental and economic factors are low.

The GWP and unit cost, presented in Table 6, were calculated as follows: The GWP of the concrete was estimated by its respective CO₂ emissions. The unit cost of each concrete mixture was computed based on the individual costs of the raw materials.

Fig. 20 show that the concrete mixes with the secondary and ternary blends showed higher efficiency factors than their counterparts with only cement, where 60C25F15M yielded the highest efficiency factor. In this system, the engineering performance was better because, although the compressive strength and workability were worse than at 100 C, they do not counteract the effect of the great improvement in durability. Further, although the cost factor of the system was worse than the cost of 100 C but, this negative factor was highly balanced by better engineering performance and considerably better environmental performance.

The system 75C25F shows a very good workability factor and a medium durability performance; however, the poor compressive

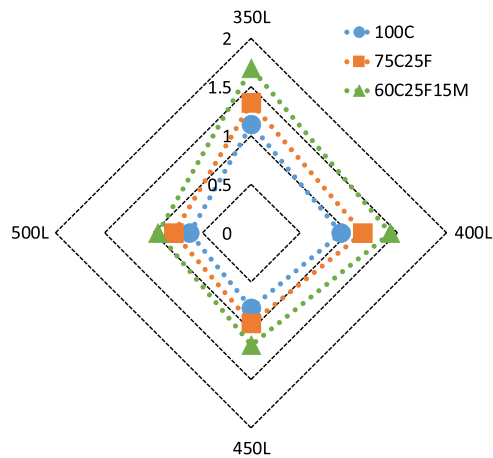


Fig. 20. ME results.

strength results in this system presenting a worse engineering factor. Further, its cost is the lowest, and its environmental behavior is in the middle of the three systems. Thus, this system showed better material efficiency than 100 C but worse than 60C25F15M.

6. Conclusions

This study analyzed the influence of two SCMs (limestone filler and metakaolin) on the rheological properties and hardened state of SCC using four paste volume levels (350–400–450–500 l). Three paste compositions were designed: one with only cement (100 C), one replacing cement with 25% limestone filler (75C25F), and the last replacing cement with 25% limestone filler and 15% metakaolin (60C25F15M).

The results lead to state that the use of limestone in binary binders (75C25F) results in a reduction in both the yield stress and plastic viscosity as it dismisses the number of flocculated cement particles. However, owing to the high specific surface area, the inclusion of metakaolin in ternary binders (60C25F15M) counteracts this effect and increases the rheological parameters. The increase in the solid volume fraction (reducing the paste volume) increases the rheological parameters and modifies the slump flow results accordingly.

In hardened state, the employment of SCM reduces both UPV and strength, with the reduction in 75C25F being higher than that in 60C25F15M. In addition, the evolution of the UPV in the first 20 days of 60C25F15M was higher than that of the other systems. Both of these issues were because of the pozzolanic reaction of metakaolin. In this hardened state, the mechanical performance decreased as the paste content increased, which is attributed to the mortar thickness coating the aggregates.

The best durability performance is shown by concretes with ternary binder, 60C25F15M. The use of limestone filler and particularly metakaolin, reduces the volume of voids in the cement paste and, in the latter case, contributes to its densification, producing a pore structure refinement after pozzolanic activity that will enhance the durability performance.

Finally, to measure the efficiency of the concrete, a material index was designed that considered the fresh behavior, mechanical performance, durability, cost, and environmental impact. SCCs with ternary binders (60C25F15M) provided the highest indices. Thus, the use of alternative materials, particularly metakaolin, in the design of SCC has been proven to be a good option to optimize its sustainable performance.

Declaration of Competing Interest

The authors declare that they have no known competing financial interests or personal relationships that could have appeared to influence the work reported in this paper.

Acknowledgements

The study is part of two projects entitled: “Robust self-compacting recycled concretes: rheology in fresh state and mechanical properties (Ref: BIA2014-58063-R)” and “Sustainable High Performance Self-Compacting Concrete using low clinker cement, and integral curing and self-healing agents (HACCURACEM) (BIA2017-85657-R)” funded by MINECO.

Moreover, this work was also made possible by the financial support of a pre-doctoral grant of MINECO (FPI 2015- ref BES-2015-071919) and two grants for international pre-doctoral stays: (a) FPI 2015 and (b) IACOBUS program for “Galicia–North of Portugal Euroregion”.

References

- [1] M.T. Marvila, A.R.G. de Azevedo, P.R. de Matos, S.N. Monteiro, C.M.F. Vieira, Materials for production of high and ultra-high performance concrete: review and perspective of possible novel materials, *Materials* 14 (2021) 4304, <https://doi.org/10.3390/ma14154304>.
- [2] K. Holschemacher, Hardened material properties of self-compacting concrete, *J. Civ. Eng. Manag.* 10 (2004) 261–266, <https://doi.org/10.1080/13923730.2004.9636318>.
- [3] P.L. Domone, A review of the hardened mechanical properties of self-compacting concrete, *Cem. Concr. Compos.* 29 (2007) 1–12, <https://doi.org/10.1016/j.cemconcomp.2006.07.010>.
- [4] P. Van den Heede, N. De Belie, Environmental impact and life cycle assessment (LCA) of traditional and 'green' concretes: Literature review and theoretical calculations, *Cem. Concr. Compos.* 34 (2012) 431–442, <https://doi.org/10.1016/j.cemconcomp.2012.01.004>.
- [5] M. Gesoğlu, E. Güneysi, M.E. Kocabağ, V. Bayram, K. Mermerdaş, Fresh and hardened characteristics of self compacting concretes made with combined use of marble powder, limestone filler, and fly ash, *Constr. Build. Mater.* 37 (2012) 160–170, <https://doi.org/10.1016/j.conbuildmat.2012.07.092>.
- [6] H. Zhao, W. Sun, X. Wu, B. Gao, The properties of the self-compacting concrete with fly ash and ground granulated blast furnace slag mineral admixtures, *J. Clean. Prod.* 95 (2015) 66–74, <https://doi.org/10.1016/j.jclepro.2015.02.050>.
- [7] I.P. Sfikas, E.G. Badogiannis, K.G. Trezos, Rheology and mechanical characteristics of self-compacting concrete mixtures containing metakaolin, *Constr. Build. Mater.* 64 (2014) 121–129, <https://doi.org/10.1016/j.conbuildmat.2014.04.048>.
- [8] R. Saleh Ahari, T. Kemal Erdem, K. Ramyar, Effect of various supplementary cementitious materials on rheological properties of self-consolidating concrete, *Constr. Build. Mater.* 75 (2015) 89–98, <https://doi.org/10.1016/j.conbuildmat.2014.11.014>.
- [9] S.K. Ling, A.K.H. Kwan, Adding limestone fines as cementitious paste replacement to lower carbon footprint of SCC, *Constr. Build. Mater.* 111 (2016) 326–336, <https://doi.org/10.1016/j.conbuildmat.2016.02.072>.
- [10] G. Rojo-López, S. Nunes, B. González-Fonbebo, F. Martínez-Abella, Quaternary blends of portland cement, metakaolin, biomass ash and granite powder for production of self-compacting concrete, *J. Clean. Prod.* 266 (2020), 121666, <https://doi.org/10.1016/j.jclepro.2020.121666>.
- [11] N. Careddu, G. Marras, G. Siotto, Recovery of sawdust resulting from marble processing plants for future uses in high value-added products, *J. Clean. Prod.* 84 (2014) 533–539, <https://doi.org/10.1016/j.jclepro.2013.11.062>.
- [12] K. Vance, A. Kumar, G. Sant, N. Neithalath, The rheological properties of ternary binders containing Portland cement, limestone, and metakaolin or fly ash, *Cem. Concr. Res.* 52 (2013) 196–207, <https://doi.org/10.1016/j.cemconres.2013.07.007>.
- [13] K. Vance, A. Arora, G. Sant, N. Neithalath, Rheological evaluations of interground and blended cement–limestone suspensions, *Constr. Build. Mater.* 79 (2015) 65–72, <https://doi.org/10.1016/j.conbuildmat.2014.12.054>.
- [14] M. Uysal, M. Sumer, Performance of self-compacting concrete containing different mineral admixtures, *Constr. Build. Mater.* 25 (2011) 4112–4120, <https://doi.org/10.1016/j.conbuildmat.2011.04.032>.
- [15] A. Barkat, S. Kenai, B. Menadi, E. Kadri, H. Soualhi, Effects of local metakaolin addition on rheological and mechanical performance of self-compacting limestone cement concrete, *J. Adhes. Sci. Technol.* 33 (2019) 963–985, <https://doi.org/10.1080/01694243.2019.1571737>.
- [16] K. Hornbostel, C.K. Larsen, M.R. Geiker, Relationship between concrete resistivity and corrosion rate – a literature review, *Cem. Concr. Compos.* 39 (2013) 60–72, <https://doi.org/10.1016/j.cemconcomp.2013.03.019>.
- [17] D.-H. Le, Y.-N. Sheen, M.N.-T. Lam, Fresh and hardened properties of self-compacting concrete with sugarcane bagasse ash–slag blended cement, *Constr. Build. Mater.* 185 (2018) 138–147, <https://doi.org/10.1016/j.conbuildmat.2018.07.029>.
- [18] P. Van den Heede, N. De Belie, Environmental impact and life cycle assessment (LCA) of traditional and 'green' concretes: Literature review and theoretical calculations, *Cem. Concr. Compos.* 34 (2012) 431–442, <https://doi.org/10.1016/j.cemconcomp.2012.01.004>.
- [19] A.S.E. Belaidi, S. Kenai, E.H. Kadri, H. Soualhi, B. Benchaâ, Effects of experimental ternary cements on fresh and hardened properties of self-compacting concretes, *J. Adhes. Sci. Technol.* 30 (2016) 247–261, <https://doi.org/10.1080/01694243.2015.1099864>.
- [20] J. Tang, S. Wei, W. Li, S. Ma, P. Ji, X. Shen, Synergistic effect of metakaolin and limestone on the hydration properties of Portland cement, *Constr. Build. Mater.* 223 (2019) 177–184, <https://doi.org/10.1016/j.conbuildmat.2019.06.059>.
- [21] G. Medjigbodo, E. Rozière, K. Charrier, L. Izoret, A. Loukili, Hydration, shrinkage, and durability of ternary binders containing Portland cement, limestone filler and metakaolin, *Constr. Build. Mater.* 183 (2018) 114–126, <https://doi.org/10.1016/j.conbuildmat.2018.06.138>.
- [22] K. Vance, M. Aguayo, T. Oey, G. Sant, N. Neithalath, Hydration and strength development in ternary portland cement blends containing limestone and fly ash or metakaolin, *Cem. Concr. Compos.* 39 (2013) 93–103, <https://doi.org/10.1016/j.cemconcomp.2013.03.028>.
- [23] M. Mahdikhani, A.A. Ramezani-pour, New methods development for evaluation rheological properties of self-consolidating mortars, *Constr. Build. Mater.* 75 (2015) 136–143, <https://doi.org/10.1016/j.conbuildmat.2014.09.094>.
- [24] I. Navarrete, Y. Kurama, N. Escalona, M. Lopez, Impact of physical and physicochemical properties of supplementary cementitious materials on structural build-up of cement-based pastes, *Cem. Concr. Res.* 130 (2020), <https://doi.org/10.1016/j.cemconres.2020.105994>.
- [25] R. Madandoust, S.Y. Mousavi, Fresh and hardened properties of self-compacting concrete containing metakaolin, *Constr. Build. Mater.* 35 (2012) 752–760, <https://doi.org/10.1016/j.conbuildmat.2012.04.109>.
- [26] F. Cassagnabère, P. Diederich, M. Mouret, G. Escadeillas, M. Lachemi, Impact of metakaolin characteristics on the rheological properties of mortar in the fresh state, *Cem. Concr. Compos.* 37 (2013) 95–107, <https://doi.org/10.1016/j.cemconcomp.2012.12.001>.
- [27] NF P18-513 - Addition for concrete - Metakaolin - Specifications and conformity criteria , n.d.
- [28] M. Pavlíková, L. Zemanová, J. Pokorný, M. Záleská, O. Jankovský, M. Lojka, Z. Pavlík, Influence of wood-based biomass ash admixing on the structural, mechanical, hygric, and thermal properties of air lime mortars, *Materials* 12 (2019) 2227, <https://doi.org/10.3390/ma12142227>.
- [29] H. Hafid, G. Ovarlez, F. Toussaint, P.H. Jezuquel, N. Roussel, Effect of particle morphological parameters on sand grains packing properties and rheology of model mortars, *Cem. Concr. Res.* 80 (2016) 44–51, <https://doi.org/10.1016/j.cemconres.2015.11.002>.
- [30] EN 12350-8, 2019. Testing fresh concrete - Part 8: Self-compacting concrete - Slump-flow test, n.d.
- [31] EN 12390-3, 2019. Testing hardened concrete - Part 3: Compressive strength of test specimens, n.d.
- [32] EN 12390-6, 2009. Testing hardened concrete - Part 6: Tensile splitting strength of test specimens, n.d.
- [33] UNE 83988-2, 2014 Concrete durability. Test methods. Determination of the electrical resistivity. Part 2: Four points or Wenner method., n.d.
- [34] EFNARC, The European Guidelines for Self-Compacting Concrete, Eur. Guidel. Self Compact. Concr., 2005, 63.
- [35] A. Yahia, K. Khayat, Analytical models for estimating yield stress of high-performance pseudoplastic grout, *Cem. Concr. Res.* 31 (2001) 731–738, [https://doi.org/10.1016/S0008-8846\(01\)00476-8](https://doi.org/10.1016/S0008-8846(01)00476-8).
- [36] C. Atzeni, L. Massidda, U. Sanna, Comparison between rheological models for portland cement pastes, *Cem. Concr. Res.* 15 (1985) 511–519, [https://doi.org/10.1016/0008-8846\(85\)90125-5](https://doi.org/10.1016/0008-8846(85)90125-5).
- [37] A. Yahia, Shear-thickening behavior of high-performance cement grouts — Influencing mix-design parameters, *Cem. Concr. Res.* 41 (2011) 230–235, <https://doi.org/10.1016/j.cemconres.2010.11.004>.
- [38] B. Lorentz, N. Shanahan, A. Zayed, Rheological behavior & modeling of calcined kaolin-Portland cements, *Constr. Build. Mater.* 307 (2021), 124761, <https://doi.org/10.1016/j.conbuildmat.2021.124761>.
- [39] S. Drissi, C. Shi, N. Li, Y. Liu, J. Liu, P. He, Relationship between the composition and hydration-microstructure-mechanical properties of cement-metakaolin-limestone ternary system, *Constr. Build. Mater.* 302 (2021), 124175, <https://doi.org/10.1016/j.conbuildmat.2021.124175>.
- [40] L.G. Li, S.H. Chu, K.L. Zeng, J. Zhu, A.K.H. Kwan, Roles of water film thickness and fibre factor in workability of polypropylene fibre reinforced mortar, *Cem. Concr. Compos.* 93 (2018) 196–204, <https://doi.org/10.1016/j.cemconcomp.2018.07.014>.
- [41] S. Koliás, C. Georgiou, The effect of paste volume and of water content on the strength and water absorption of concrete, *Cem. Concr. Compos.* 27 (2005) 211–216, <https://doi.org/10.1016/j.cemconcomp.2004.02.009>.
- [42] S. Popovics, Analysis of concrete strength versus water-cement ratio relationship, *Acids Mater. J.* 87 (1990), <https://doi.org/10.14359/1944>.

- [43] F. de L, A. Belloc, The influence of aggregate on the compressive strength of normal and high-strength concrete, *Acids Mater. J.* 94 (1997), <https://doi.org/10.14359/326>.
- [44] S. Sui, W. Wilson, F. Georget, H. Maraghechi, H. Kazemi-Kamyab, W. Sun, K. Scrivener, Quantification methods for chloride binding in Portland cement and limestone systems, *Cem. Concr. Res.* 125 (2019), 105864, <https://doi.org/10.1016/j.cemconres.2019.105864>.
- [45] S. Demirhan, K. Turk, K. Ulugerger, Fresh and hardened properties of self consolidating Portland limestone cement mortars: effect of high volume limestone powder replaced by cement, *Constr. Build. Mater.* 196 (2019) 115–125, <https://doi.org/10.1016/j.conbuildmat.2018.11.111>.
- [46] A.A. Ramezaniapour, E. Ghiasvand, I. Nickseresht, M. Mahdikhani, F. Moodi, Influence of various amounts of limestone powder on performance of Portland limestone cement concretes, *Cem. Concr. Compos.* 31 (2009) 715–720, <https://doi.org/10.1016/j.cemconcomp.2009.08.003>.
- [47] J. Langford, P. Broomfield, *Monitoring the Corrosion of Reinforcing Steel*, Palladian Publications Ltd, 1987.
- [48] A.E. Landa-Gómez, R. Croche B, S. Márquez-Montero, R. Galván-Martínez, C.G. Tiburcio, F.A. Calderón, M.A. Baltazar-Zamora, Correlation of compression resistance and rupture module of a concrete of ratio w/c = 0.50 with the corrosion potential, electrical resistivity and ultrasonic pulse speed, *ECS Trans.* 84 (2018) 217–227, <https://doi.org/10.1149/08401.0217ecst>.
- [49] A. Bagheri, H. Zanganeh, H. Alizadeh, M. Shakerinia, M.A.S. Marian, Comparing the performance of fine fly ash and silica fume in enhancing the properties of concretes containing fly ash, *Constr. Build. Mater.* 47 (2013) 1402–1408, <https://doi.org/10.1016/j.conbuildmat.2013.06.037>.
- [50] A. Sadrmomtazi, B. Tahmouresi, A. Saradar, Effects of silica fume on mechanical strength and microstructure of basalt fiber reinforced cementitious composites (BFRCC), *Constr. Build. Mater.* 162 (2018) 321–333, <https://doi.org/10.1016/j.conbuildmat.2017.11.159>.
- [51] ISO 14067, 2018(en), Greenhouse gases — Carbon footprint of products — Requirements and guidelines for quantification, n.d.
- [52] R. Zhong, K. Wille, R. Viegas, Material efficiency in the design of UHPC paste from a life cycle point of view, *Constr. Build. Mater.* 160 (2018) 505–513, <https://doi.org/10.1016/j.conbuildmat.2017.11.049>.
- [53] B. Chiaia, A.P. Fantilli, A. Guerini, G. Volpatti, D. Zampini, Eco-mechanical index for structural concrete, *Constr. Build. Mater.* 67 (2014) 386–392, <https://doi.org/10.1016/j.conbuildmat.2013.12.090>.
- [54] H.S. Müller, M. Haist, M. Vogel, Assessment of the sustainability potential of concrete and concrete structures considering their environmental impact, performance and lifetime, *Constr. Build. Mater.* 67 (2014) 321–337, <https://doi.org/10.1016/j.conbuildmat.2014.01.039>.
- [55] Z. Abdollahnejad, S. Miraldo, F. Pacheco-Torgal, J.B. Aguiar, Cost-efficient one-part alkali-activated mortars with low global warming potential for floor heating systems applications, *Eur. J. Environ. Civ. Eng.* 21 (2017) 412–429, <https://doi.org/10.1080/19648189.2015.1125392>.